materials

MDPI

Article

Monolithic Multicolor Emissions of InGaN-Based Hybrid Light-Emitting Diodes Using $CsPbBr_3$ Green Quantum Dots

Jae-Hyeok Oh [1], Seung-Beom Cho [2], Il-Kyu Park [2] and Sung-Nam Lee [1,3,*]

[1] Department of IT & Semiconductor Convergence Engineering, Tech University of Korea, Siheung 15073, Republic of Korea
[2] Department of Materials and Science Engineering, Seoul National University of Science & Technology, Seoul 01811, Republic of Korea
[3] Department of Nano & Semiconductor Engineering, Tech University of Korea, Siheung 15073, Republic of Korea
* Correspondence: snlee@tukorea.ac.kr; Tel.: +82-31-8041-0721

Abstract: To address the increasing demand for multicolor light-emitting diodes (LEDs), a monolithic multicolor LED with a simple process and high reliability is desirable. In this study, organic–inorganic hybrid LEDs with violet and green wavelengths were fabricated by depositing $CsPbBr_3$ perovskite green quantum dots (QDs) as the light-converting material on InGaN-based violet LEDs. As the injection current was increased, the total electroluminescence (EL) intensities of the hybrid LEDs increased, whereas the light-converted green emission efficiency of the $CsPbBr_3$ QDs decreased. The maximum green-to-violet EL spectral intensity ratio of the hybrid LEDs with $CsPbBr_3$ QDs was achieved with the injection current of <10 mA. Moreover, the EL spectral ratio of the green-to-violet emission decreased at an injection current of 100 mA. The light-conversion intensity of the $CsPbBr_3$ QDs decreased linearly as the junction temperature of the hybrid LEDs was increased with increasing injection current, similar to the temperature-dependent photoluminescence degradation of $CsPbBr_3$ QDs. In addition, the junction temperature of the hybrid LED was minimized by pulse injection to suppress the thermal degradation of QDs and increase the light conversion efficiency to green emission. Therefore, the overall emission spectrum color coordinates of the hybrid LEDs exhibited a red shift from violet to blue in the low-current region and a blue shift toward violet as the green emission of the QDs was decreased above 10 mA.

Keywords: multicolor emission; InGaN; hybrid light-emitting diode; $CsPbBr_3$; quantum dot; light conversion; injection current

Citation: Oh, J.-H.; Cho, S.-B.; Park, I.-K.; Lee, S.-N. Monolithic Multicolor Emissions of InGaN-Based Hybrid Light-Emitting Diodes Using $CsPbBr_3$ Green Quantum Dots. *Materials* **2023**, *16*, 1290. https://doi.org/10.3390/ma16031290

Academic Editor: Johann Bouclé

Received: 4 January 2023
Revised: 28 January 2023
Accepted: 1 February 2023
Published: 2 February 2023

1. Introduction

The development of multicolor light-emitting diodes (LEDs) is promising for multifunctional lighting sources, such as display, biomedical, agricultural, and cosmetic applications [1–3]. To fabricate a multifunctional lighting source, two or three individual LEDs are integrated to realize dichromatic or trichromatic multicolor LEDs [1,4]. However, as multicolor LEDs use two kinds of LED and additional integration technology, the device reliability is lower than that of monolithic multicolor LEDs, and the fabrication process is more complicated [5,6]. Therefore, a monolithic multicolor LED with a simple process and high reliability for various applications is desirable.

Recently, III-nitride semiconductors have garnered considerable attention as the most common visible light-emitting materials that can achieve stable wavelengths by controlling the compositions of ternary or quaternary compound semiconductors [7,8]. In particular, InGaN ternary semiconductors have been widely used as blue and green light sources by controlling the In composition of the InGaN active layer [7]. Therefore, InGaN-based monolithic LEDs have been fabricated by the growth of dual-emission InGaN active layers, such as self-organized InGaN quantum dots (QDs) and blue/yellow dual InGaN quantum

wells (QWs), using different In compositions and well thicknesses [9–11]. However, high-efficiency green and blue emissions cannot be easily simultaneously achieved from InGaN-based LEDs because of the In segregation and large lattice mismatch [12–14].

To address the limitations of InGaN-based monolithic LEDs, high-efficiency InGaN-based LEDs with light-conversion materials, such as $CuInS_2$, yttrium aluminum garnet (YAG), and silicate-based phosphors, have garnered attention for the fabrication process [15–17]. $CuInS_2$ exhibits a wide half-width, making it suitable as a light-converting device for lighting sources, whereas YAG- and silicate-based phosphors have low color purity and reliability, which are not suitable for multiwavelength LEDs [15–17]. CdSe–ZnS nanocrystals, which adsorb high-energy blue emissions generated from InGaN-based LEDs, have been reported to convert low-energy green or yellow emissions [18].

Recently, perovskite QDs have been studied to improve light-conversion efficiency due to their Cd-free properties [19,20]. In particular, $CsPbBr_3$ perovskite QDs are superior to conventional QD materials because of their high light absorption coefficient and stability [19–21]. In addition, $CsPbBr_3$ QDs have a pure green photoluminescence (PL) emission of approximately 520 nm with a narrower bandwidth and higher quantum efficiency of ~90% [21]. Thus, $CsPbBr_3$ QDs are considered as candidates for realizing converted green emissions using high-energy emission LEDs because of their absorption and emission properties. In particular, hybrid LEDs combining green $CsPbBr_3$ and blue-violet InGaN-based LEDs are expected to achieve a multiwavelength LED that can control a wide range of emission wavelengths from blue-violet to green by controlling the conversion efficiency.

In this study, organic–inorganic hybrid LEDs with a mixed violet and green wavelength range were fabricated by depositing $CsPbBr_3$ perovskite green QDs as the light-converting material on InGaN-based violet LEDs. The light-conversion performance of the materials was tested under different injection currents and temperatures.

2. Materials and Methods

$CsPbBr_3$ QDs were synthesized using a modified hot injection method [22,23]. Briefly, 325 mg Cs_2CO_3 dissolved in a mixture of 1 mL oleic acid and 3 mL 1-octadecene was vacuum-dried in a three-neck flask at 100 °C for 30 min to synthesize the Cs-oleate solution. In another flask, 138 mg $PbBr_2$ was dissolved in a mixture of 1 mL oleic acid, 1 mL oleylamine, and 10 mL 1-octadecene. The solution was vacuum dried in a three-neck flask at 120 °C for 30 min and heated to 180 °C. Subsequently, 1 mL Cs-oleate solution was injected into the reaction flask. After 7 s, the reaction flask was dipped into an ice-water bath to stop the reaction. To remove the unreacted white solid and excess ligand residues, the crude solution was centrifuged at 10,000 rpm for 3 min. The QD inks were washed with ethyl acetate with a volume ratio of 3:1, followed by re-precipitation to produce a pure colloidal QD solution. Then, the QDs were re-dispersed into an *n*-octane solution for further use.

The InGaN-based LED epitaxial structure was grown on a c-plane (0001) sapphire substrate using metal–organic chemical deposition. Trimethylgallium, trimethylindium, trimethylaluminum, and ammonia were used as Ga, In, Al, and N precursors, respectively. The InGaN-based violet LEDs consisted of 4.0 μm-thick Si-doped n-GaN, five-period $In_{0.1}Ga_{0.9}N$/GaN QWs, 20 nm-thick p-AlGaN electron-blocking layer, and 0.1 μm-thick Mg-doped p-GaN. The growth temperatures of n-type and p-type GaN films are 1030 and 900 °C, respectively. As the active layer, InGaN/GaN 5-QW structures composed of 3.0 nm-thick $In_{0.1}Ga_{0.9}N$ wells and 10.0 nm-thick GaN barriers were grown at 800 °C. Subsequently, LED chips with lateral electrode structures were fabricated using a conventional mesa LED process. After depositing the Ni/Au p-electrode on the LEDs, $CsPbBr_3$ QDs were deposited on the InGaN-based violet LEDs using a spin-coating process. For the spin-coating method, 50 μL $CsPbBr_3$ was added at 2000 rpm for 60 s, and then the n-hexane solvent was removed at 70 °C for 20 min in a nitrogen atmosphere.

The microstructure of the $CsPbBr_3$ QDs was observed using a transmission electron microscope (TEM, JEOL-2010, Tokyo, Japan) at 200 kV. To measure the TEM, 10 μL of

$CsPbBr_3$ QD solution was dropped onto the copper grid. They were dried in a vacuum oven at 60 °C for 30 min to remove the organic substances, which could interrupt a clear TEM image. The surface structures of the $CsPbBr_3$ QDs on glass, InGaN-based LEDs and hybrid LEDs were measured using noncontact mode atomic force microscopy (AFM). Optical absorption and transmittance of the $CsPbBr_3$ QDs on glass and InGaN-based LEDs were obtained using UV-visible spectroscopy. In addition, the optical emission properties of the $CsPbBr_3$ QDs, InGaN-based violet LEDs, and hybrid LEDs were evaluated by room-temperature PL measurements using a 266 nm laser. To observe the effects of QD deposition on the current, voltage, and emission intensity of the hybrid LEDs, light output power (L)–current (I)–voltage (V) measurements were carried out using an HP4155A parameter analyzer with a 918D-UV-OD3R Newport photodetector capable of current injection and photocurrent measurements. In addition, electroluminescence (EL) spectra of LEDs were obtained by USB 4000 fiber optic spectrometer. The junction temperature of the hybrid LEDs was measured using the forward voltage method [24]. In addition, temperature-dependent PL measurements at 25–100 °C were performed using a hot chuck and 405 nm laser as the excitation source to observe the optical and thermal damage of the $CsPbBr_3$ QDs.

3. Results and Discussion

Figure 1a shows images of the $CsPbBr_3$ QDs on a glass substrate, InGaN-based violet LEDs, and hybrid InGaN-based multicolor LEDs with $CsPbBr_3$ QDs. Detailed 3-dimensional schematic diagrams of QDs on glass, InGaN-based violet LED, and hybrid LED structures are described in Figure S1. $CsPbBr_3$ on glass exhibits excellent transparency and a light green color. The hybrid InGaN-based LEDs have a darker yellow color than that of conventional InGaN-based violet LEDs, which was obtained by depositing $CsPbBr_3$ QDs. This indicates that $CsPbBr_3$ QDs can be uniformly coated on the glass substrates and InGaN-based LEDs by spin coating. Figure 1b,c show the TEM images of the synthesized all-inorganic $CsPbBr_3$ QDs, which exhibited a uniform cubic shape. The black dot spots shown in higher-resolution TEM image has been known as metallic Pb particle formed by electron beam exposure [25]. The $CsPbBr_3$ QDs have an average size of approximately 8.7 nm with a uniform size distribution. As the size of the QDs was slightly larger than the bulk exciton Bohr radius of 7 nm, the PL spectra did not show a blue shift due to the quantum confinement effect [26]. In addition, the $CsPbBr_3$ QDs were well dispersed in the *n*-octane solution without agglomeration. This indicates that the ligand functional groups of the QDs helped stabilize the colloidal stability, thereby allowing them to be spin-coated on other surfaces, such as sapphire or GaN LED chips.

From the AFM analysis, the average surface grain size and root mean square roughness (RMS) of the $CsPbBr_3$ QDs on the glass substrate was measured to be approximately 50 and 23 nm, respectively, as shown in Figure 1d. This indicates that spin coating technology is a useful deposition method that can form $CsPbBr_3$ QD-coated thin films with a uniform smooth surface. Figure 1e shows the AFM surface morphology of the GaN-based violet LED with a smooth step-like and hillock surface structure, which is a typical surface morphology of GaN films [27]. This suggests the smooth surface structure of the GaN-based LEDs with an RMS surface roughness of 0.6 nm. After coating the $CsPbBr_3$ QDs on the InGaN-based LEDs, the surface structure of the hybrid LEDs was significantly changed from a step-like surface to a granular spherical surface, as shown in Figure 1f. The RMS roughness of the hybrid InGaN-based LED coated with $CsPbBr_3$ QDs was 26 nm, which is almost the same as that of the $CsPbBr_3$ QDs on glass. This suggests that $CsPbBr_3$ QDs can be coated on InGaN-based LED and glass substrates.

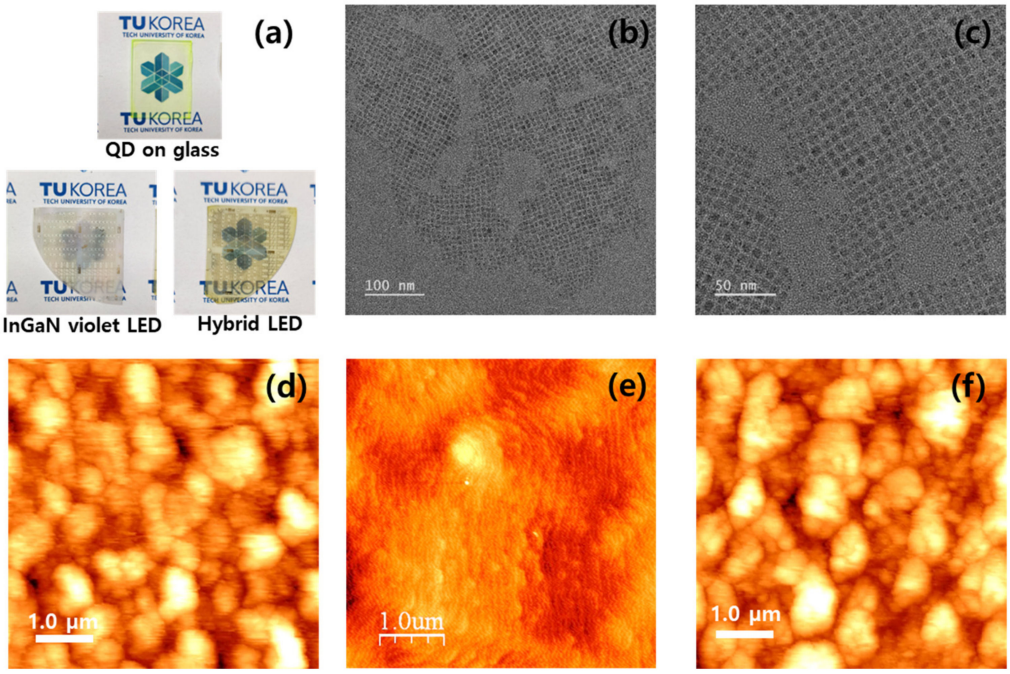

Figure 1. (**a**) Images of spin-coated $CsPbBr_3$ on glass, conventional InGaN-based violet LEDs, and hybrid LED with $CsPbBr_3$ QDs. (**b**,**c**) TEM images of the $CsPbBr_3$ QDs. Surface morphologies of (**d**) spin-coated $CsPbBr_3$ on glass, (**e**) InGaN-based violet LED, and (**f**) hybrid LED with $CsPbBr_3$ QDs obtained by AFM.

Figure 2a shows the room-temperature PL and light absorption spectra of the $CsPbBr_3$ QDs deposited on a glass substrate. The bandgap energy of the $CsPbBr_3$ QDs can be estimated at the light-absorption edge to be ~2.390 eV, which is approximately equal to the emission energy (~2.391 eV) of the PL peak. The $CsPbBr_3$ QDs exhibit a small Stokes shift, indicating that green QDs have excellent uniform optical properties. In addition, the full width at half maximum (FWHM) of the $CsPbBr_3$ QDs PL spectrum was measured to be ~60 meV, which exhibits uniform green emission characteristics compared to the InGaN-based LED. Figure 2b shows the PL and light-absorption spectra of the InGaN-based violet LED. A sharp absorption edge was measured at 3.380 eV, corresponding to the GaN template. A significant change in the absorption coefficient corresponding to the InGaN active layer was observed at 3.095 eV. Moreover, the PL peak energy of the InGaN-based LED was approximately 3.024 eV, which exhibits a Stokes shift of approximately 71 meV from the bandgap of the InGaN active layer obtained by light absorption. This can be ascribed to the slightly non-uniform In composition or well thickness in the five-period InGaN/GaN QW structure. Figure 2c shows the PL spectra of the hybrid LED with $CsPbBr_3$ QDs as the light converter. Two strong peaks at 410 and 517 nm were observed for the hybrid InGaN-based LED with $CsPbBr_3$ QDs. From Figure 2a,b, emissions at 410 and 518 nm were noted from the violet InGaN active layer and $CsPbBr_3$ green QDs, respectively. The PL intensity of the $CsPbBr_3$ green QDs was 20% higher than that of the InGaN-based violet LEDs. However, no evidence pertains to the superior optical quality of the $CsPbBr_3$ QDs to that of the InGaN-based LEDs. As the excitation light source first excited the upper green QDs on the LED and passed through the p-GaN upper layer to excite the InGaN active layer, the violet emission of the InGaN active layer is lower than the green QD emission. However, the $CsPbBr_3$ QDs were coated sufficiently well to emit green emissions by exciting a high-energy light source on InGaN-based LED using a spin-coating process.

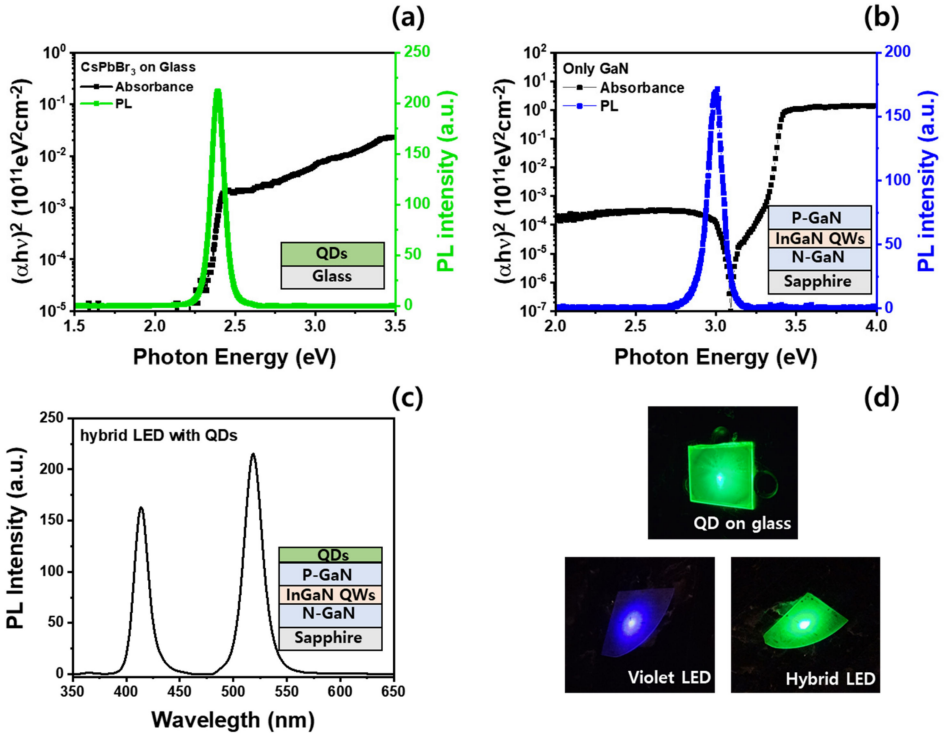

Figure 2. Room-temperature PL and absorption spectra of (**a**) spin-coated $CsPbBr_3$ QDs on glass, (**b**) conventional InGaN-based LED, and (**c**) hybrid InGaN-based LED using $CsPbBr_3$ QD; (**d**) images of the PL emissions obtained from the spin-coated $CsPbBr_3$ QDs on glass, conventional InGaN-based LED, and hybrid InGaN-based LED using $CsPbBr_3$ QDs.

Figure 3a shows the I–V characteristics of the conventional InGaN-based violet LED and hybrid LEDs with $CsPbBr_3$ QDs. The threshold and operation voltages for both LEDs are 2.7 and 3.2 V, respectively. In addition, the log-scaled I–V curves of the two LEDs have identical forward and reverse electrical characteristics, as shown in the inset of Figure 3a. This indicates that the spin-coating process of the $CsPbBr_3$ QDs proceeded well without electrical damage to the violet LED because the $CsPbBr_3$ QDs were coated after the p-type electrode deposition of the LED was formed. However, the light output powers of a conventional InGaN-based violet LED and hybrid LED coated with $CsPbBr_3$ QDs are similar in the low-current region (<10 mA), whereas the light output power of the hybrid LED using $CsPbBr_3$ QDs is slightly lower than that of conventional InGaN-based violet LED in the high-current region (>20 mA), as shown in Figure 3b. The difference in the light output power between the two LEDs at an injection current of 5.0 mA was less than 3.0%. However, when a current of 100 mA was injected, the light output power of the hybrid LED was 90.4% that of the InGaN-based violet LEDs, as shown in the inset of Figure 3b. The external quantum efficiencies (EQE) of the InGaN-based violet LEDs and hybrid LEDs with $CsPbBr_3$ QDs showed a typical efficiency droop with maximum values of 38.8% and 35.6% at 20 mA, respectively, as shown in Figure 3c. This indicates that the EQE of the InGaN-based violet LEDs decreased by coating with $CsPbBr_3$ QDs. In particular, the EQE of the InGaN-based violet LEDs was higher than that of the hybrid LEDs under an injection current of more than 10 mA because of the light conversion efficiency of the $CsPbBr_3$ QDs under the excitation light (~410 nm) of the InGaN-based violet LEDs. Above the maximum EQE of 20 mA, the EQE reduction ratio of the InGaN-based violet LEDs to the hybrid LEDs was proportional to the injection current, as shown in Figure 3d. This indicates that the light conversion efficiency of the $CsPbBr_3$ QDs decreased proportionally with the injection current. The optical properties of $CsPbBr_3$ perovskite QDs with an ABX_3 structure are vulnerable to moisture and heat due to oxygen diffusion and structural decomposition [28,29]. Hence, the heat generated by the InGaN-based violet LEDs under a

high injection current is expected to deteriorate the light conversion efficiency of $CsPbBr_3$ QDs, resulting in an EQE decrease in the hybrid LEDs.

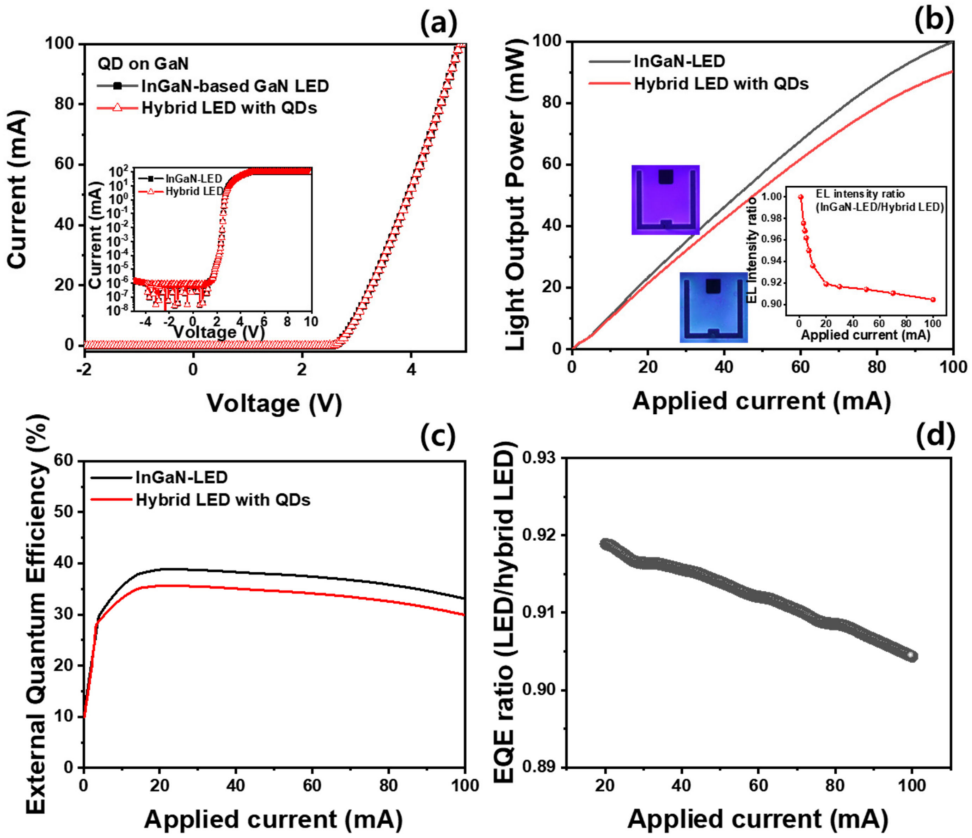

Figure 3. L–I–V characteristics of the InGaN-based and hybrid LEDs: (**a**) I–V curves, (**b**) light output power versus injection current, and (**c**) EQE of InGaN-based violet LED and hybrid LED with $CsPbBr_3$ QDs; (**d**) EQE ratio of InGaN-based violet LEDs to hybrid LEDs with $CsPbBr_3$ QDs as a function of the injection current.

To analyze the decrease in the light output power in the region with a high injection current of the hybrid LEDs, the normalized EL of the hybrid LEDs was investigated as the injection current was increased from 0.1 to 100 mA, as illustrated in Figure 4a. Two main EL peaks were noted: violet emission (410 nm) from the InGaN active region and green emission (518 nm) from $CsPbBr_3$ QDs. The EL intensity of the $CsPbBr_3$ green QD emission was approximately 20% that of the violet GaN-based LEDs, indicating that the light-conversion efficiency of $CsPbBr_3$ QDs is still low for the violet emission of InGaN-based LEDs. As the injection current was increased to 10 mA, the EL spectrum of the $CsPbBr_3$ QDs initially increased and then rapidly decreased above 10 mA. To observe the effect of the injection current on the violet-to-green emissions of the hybrid LEDs, the EL intensity ratio of the green-to-blue-violet emissions was plotted as a function of the injection current, as shown in Figure 4b. The EL intensity ratio of green to violet emission increased to 21.6% at 5.0 mA and decreased to 12.6% at 100 mA. Thus, the maximum light conversion efficiency of the $CsPbBr_3$ QDs for the violet excitation emission source was noted at a low injection current of 5.0 mA, which decreased in the high-injection-current region. From the different conversion efficiencies of the $CsPbBr_3$ QDs shown in the insets of Figure 4b, the hybrid LEDs using $CsPbBr_3$ QDs exhibit a bluish-green emission in the low-current region and violet emission in the high-current region. As the device temperature of LEDs increases with the injection current due to an increase in the junction temperature [30], we measured the junction temperature of the hybrid LED using the forward-voltage method [24]. As the injection current was increased from 10 mA to 100 mA, the junction temperature of the hybrid LEDs increased from 26.2 °C to 65 °C, as shown in Supplementary S2. This indicates

that the hybrid LEDs have good epitaxial properties with low nonradiative recombination centers, which can generate heat in the junction region. However, the light-conversion efficiency of the $CsPbBr_3$ QDs may be deteriorated by thermal degradation due to the increased junction temperature of the hybrid LEDs.

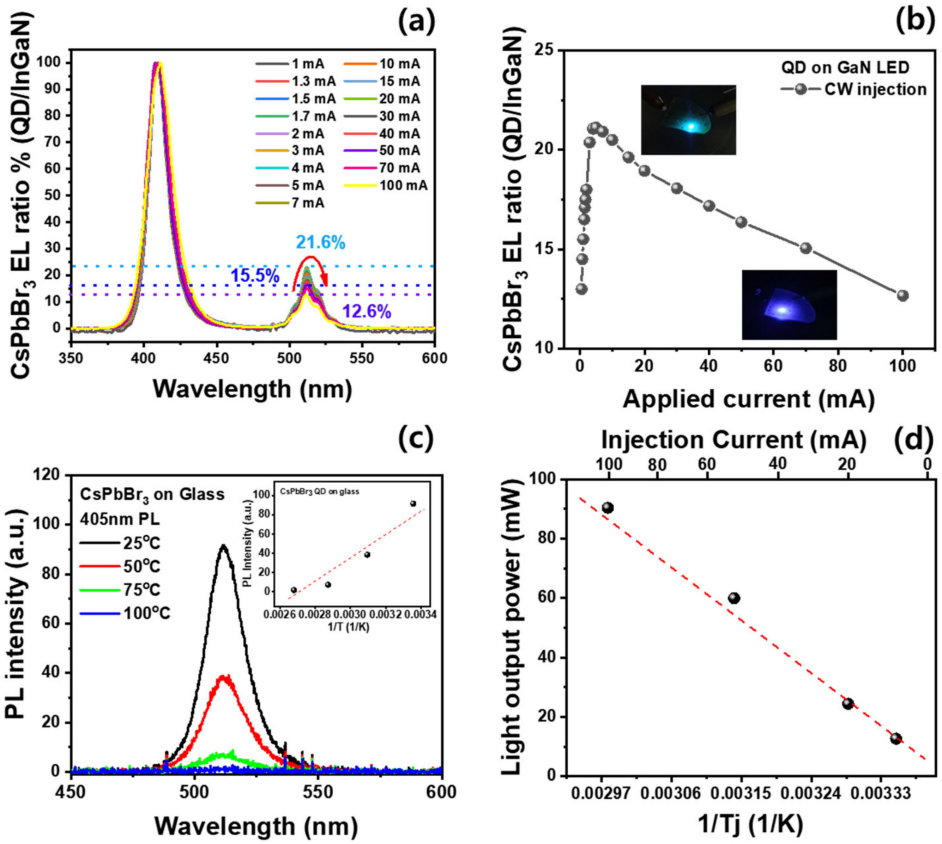

Figure 4. (**a**) Normalized EL spectra of the hybrid LEDs with $CsPbBr_3$ QDs under different injection currents. (**b**) EL intensity ratio of the green to violet emissions in hybrid LEDs. (**c**) Temperature-dependent PL spectra of the $CsPbBr_3$ QDs on glass substrate. The inset is the PL intensity of the $CsPbBr_3$ QDs as a function of reciprocal temperature. (**d**) The light output power of the hybrid LEDs as a function of the reciprocal junction temperature and injection current.

To investigate the effect of thermal degradation on the optical properties of $CsPbBr_3$ QDs, temperature-dependent PL analysis was performed on $CsPbBr_3$ QDs at 25–100 °C, as shown in Figure 4c. The PL intensity of the $CsPbBr_3$ QDs significantly decreased with increasing ambient temperature. By using the Arrhenius equation [31], the activation energy for the temperature-dependent decrease in the PL intensity was calculated to be 50.4 meV, as shown in the inset of Figure 4c. The junction temperature of the hybrid LEDs is proportional to the injection current, as shown in Supplementary S2. By using the junction temperature of the hybrid LEDs, the EL intensity was plotted as a function of the junction temperature to calculate the activation energy for the temperature-dependent EL intensity of the hybrid LEDs, as shown in Figure 4d. The activation energy of the temperature-dependent EL intensity of the hybrid LEDs was calculated to be 44.5 meV, which is similar to that of the $CsPbBr_3$ QDs. Therefore, the decrease in the EL intensity of the hybrid LEDs with increasing current can be explained by the thermal degradation of the QDs, such as the oxygen diffusion and decomposition of the unstable colloidal structure on the QD surface [29], as the temperature of the hybrid LEDs increased with the junction temperature.

Figure 5a,b show the EL spectra of the hybrid LEDs with $CsPbBr_3$ QDs with different injection currents using the continuous-wave (CW) and pulse injection conditions,

respectively. Under both conditions, the violet emission of the InGaN active layer is higher than that of the $CsPbBr_3$ QDs. The blue-violet emission (~410 nm) exhibits a redshift with increasing continuous current injection due to the thermal heating-induced band gap shrinkage effect, whereas no redshift phenomenon was noted under the high-pulse-injection condition [32]. The FWHMs of the violet and green EL spectra obtained by the CW operation are wider than those obtained by the pulse operation, which confirms the thermal heating effect [33]. Figure 5c shows the EL integrated intensities of the violet and green emission spectra generated from the hybrid LEDs as a function of the CW and pulse injection currents. The CW EL intensity of the violet emission generated from the InGaN active layer was slightly lower than that under the pulse-injection condition. However, the CW EL intensity of the green emission from the $CsPbBr_3$ QDs did not further increase above 50 mA, whereas that of the green QDs measured under pulse conditions increased almost linearly with the injection current. The EL intensity ratio of the green-to-violet emission measured under the CW and pulse injection conditions in the hybrid LEDs is shown in Figure 5d. For the CW condition, the maximum intensity ratio (21.1%) of the green to violet emission was obtained at 5.0 mA, which rapidly decreased with increasing injection current. However, the intensity ratio of the green emission to the blue-violet emission did not decrease until the pulse injection current was 100 mA. As a result, the emission intensity ratios of the green to violet LED emission measured under CW and pulse injection conditions were 12.6% and 22.8% at 100 mA, respectively. In addition, it is observed that the green emission intensity of the hybrid LED operated by pulse operation is much more stable than that of cw operation, as shown in Supplementary S3. Hence, the decrease in the emission efficiency of hybrid LEDs at high operation currents is attributed to the reduction in the light conversion efficiency of the $CsPbBr_3$ green QDs due to thermal degradation such as oxygen diffusion and decomposition of unstable colloidal structure with increasing junction temperature of hybrid LEDs [29,34].

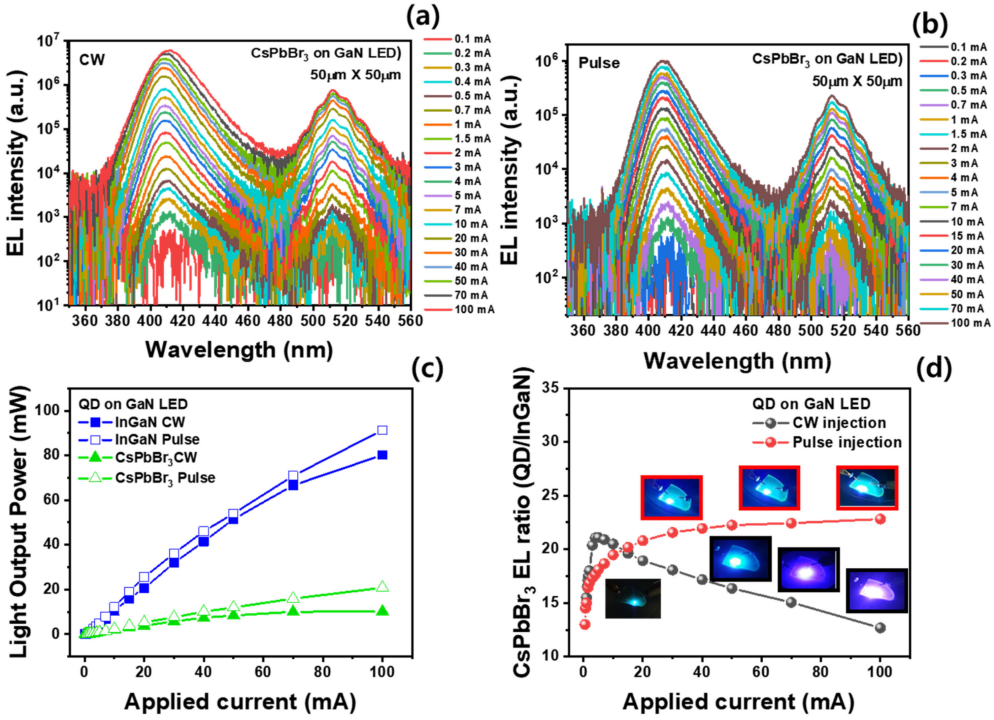

Figure 5. EL spectra of the hybrid LEDs with $CsPbBr_3$ QDs with different (**a**) CW and (**b**) pulse injection (pulse width 5.0 μs and 1.0 % duty cycle) currents; (**c**) EL spectral intensity of the violet InGaN active layer and green $CsPbBr_3$ QDs in the hybrid LEDs as a function of the CW and pulse injection currents; (**d**) EL intensity ratio of the green to violet emission in the hybrid LEDs with different CW and pulse injection currents.

The insets of Figure 5d show the emission images of the hybrid LED wafer with different CW and pulse injection currents. The hybrid LEDs emit blue-based emissions in all pulse injection regions, and blue emissions followed by violet emission as the CW injection current was increased because of the decrease in the green emission. This indicates that the hybrid LEDs can emit various color coordinates due to the change in the emission intensity ratio of the violet to green emission under the CW and pulse injection conditions.

Figure 6a,b show the color coordinates of the EL spectra of the hybrid LEDs with different CW and pulse injection conditions, respectively. Under the CW injection condition, the color coordinates of (0.1206, 0.1731) of the hybrid LEDs were obtained at a low injection current of 0.5 mA. As the injection current was increased, the color coordinate of the hybrid LED shifted to the green emission point of (0.0590, 0.6914), as obtained from the $CsPbBr_3$ QDs. The maximum redshifted color coordinates of (0.1185, 0.2593) were obtained at 10 mA. The color coordinates of the hybrid LEDs shifted to the violet emission region up to 100 mA due to the rapid decrease in the light-conversion efficiency of the green $CsPbBr_3$ QDs, as shown in Figure 6a. However, as the pulse injection current was increased, the color coordinates of the hybrid LED shifted to the green emission region because of the lower thermal degradation of the light conversion efficiency of the $CsPbBr_3$ QDs. Consequently, as the injection current was increased from 10 mA to 100 mA, the color coordinates can be further redshifted from the blue emission of (0.1160, 0.2738) to the cyan emissions of (0.1187, 0.3173), as shown in Figure 6b. Based on these results, we believe that InGaN-based hybrid LEDs with $CsPbBr_3$ green QDs can achieve multicolor emissions from blue-violet to cyan emissions to minimize the thermal degradation of the light-conversion efficiency of green QDs using the pulse injection condition. In addition, the thermal and photostability of $CsPbBr_3$ QDs still remain to be improved for more applications by incorporating foreign elements, passivating the surface of QDs, or encapsulating the device.

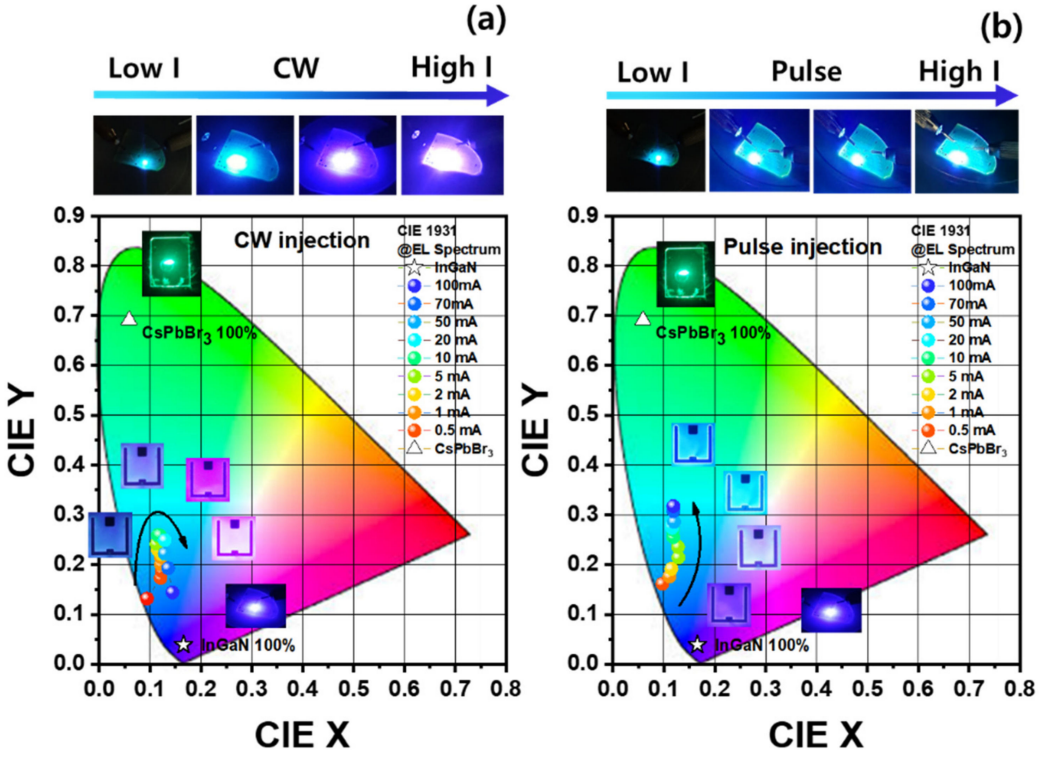

Figure 6. Color coordinate images of the hybrid LEDs using $CsPbBr_3$ QDs under (**a**) CW and (**b**) pulse injection currents. The insets are the EL images of the hybrid LED die and wafer with increasing injection currents.

4. Conclusions

In summary, multicolor InGaN-based hybrid LEDs were fabricated by depositing $CsPbBr_3$ green QDs as a light-conversion material. As the injection current was increased, the EQE of the hybrid LEDs became progressively lower than that of the InGaN-based blue-violet LEDs. Temperature-dependent PL measurements showed that the emission properties of the $CsPbBr_3$ QDs significantly deteriorated under ambient temperature. In particular, the activation energy for the temperature-dependent decrease in the EL intensity of the hybrid LEDs with green QDs was similar to that of the temperature-dependent PL intensity reduction in the green QDs. This indicates that the optical degradation of the hybrid LEDs can be ascribed to the thermal degradation of the green QDs under the high-injection-current region. To suppress the thermal degradation of the green QDs in hybrid LEDs, pulse injection can be applied to increase the emission efficiency of the hybrid LEDs with green QDs. Under the pulse injection conditions, the light-conversion efficiency of the green QDs was 22% that of the blue-violet InGaN-based LEDs under 100 mA, resulting in multicolor emissions from blue-violet to cyan.

Supplementary Materials: The following supporting information can be downloaded at: https://www.mdpi.com/article/10.3390/ma16031290/s1, Figure S1: Schematic diagrams of $CsPbBr_3$ QD on glass, InGaN-based LED and hybrid LED with $CsPbBr_3$ QDs, Figure S2: The junction temperature measurements of hybrid LED using forward voltage method. Figure S3: Green emission stability of $CsPbBr_3$ perovskite QDs in hybrid LEDs.

Author Contributions: Conceptualization, S.-N.L.; methodology, J.-H.O., S.-B.C., and I.-K.P.; software, J.-H.O.; validation, J.-H.O. and S.-N.L.; formal analysis, J.-H.O. and S.-N.L.; investigation, J.-H.O.; resources, S.-N.L.; data curation, J.-H.O. and S.-B.C.; writing—original draft preparation, J.-H.O. and I.-K.P.; writing—review and editing, S.-N.L.; visualization, J.-H.O.; supervision, S.-N.L.; project administration, S.-N.L.; funding acquisition, S.-N.L. All authors have read and agreed to the published version of the manuscript.

Funding: This research was supported by a Research Program (NRF-2020R1A2C1009630) through the National Research Foundation of Korea (NRF) funded by the Ministry of Education, Science and Technology, Republic of Korea.

Institutional Review Board Statement: Not applicable.

Informed Consent Statement: Not applicable.

Data Availability Statement: Not applicable.

Conflicts of Interest: We have no conflict of interest.

References

1. Baek, S.H.; Kim, H.W.; Lee, G.W.; Lee, S.N. Monolithic multicolor tunable inorganic light-emitting diodes. *Add. Electron. Mat.* **2021**, *8*, 2100598.
2. Yeh, N.; Chung, J.P. High-brightness LEDs-Energy efficient lighting sources and their potential indoor plant cultivation. *Renew. Sustain. Energy Rev.* **2009**, *13*, 2175–2180. [CrossRef]
3. Yeh, N.G.; Wu, C.H.; Cheng, T.C. Light-emitting diodes-Their potential in biomedical applications. *Renew. Sustain. Energy Rev.* **2010**, *14*, 2161–2166. [CrossRef]
4. Kim, H.W.; Na, Y.C.; Park, J.; Lee, S.N. Microdisk-type multicolor semipolar nitride-based light-emitting diodes. *ACS Appl. Nano. Mat.* **2022**, *5*, 9334–9343. [CrossRef]
5. Kang, C.M.; Lee, J.Y.; Kong, D.J.; Shim, J.P.; Kim, S.; Mun, S.H.; Choi, S.Y.; Park, M.D.; Kim, J.; Lee, D.S. Hybrid full-color inorganic light-emitting diodes integrated on a single wafer using selective area growth and adhesive bonding. *ACS Photon.* **2018**, *5*, 4413–4422. [CrossRef]
6. Wu, T.; Sher, C.W.; Lin, Y.; Lee, C.F.; Liang, S.; Lu, Y.; Chen, S.W.H.; Guo, W.; Kuo, H.C.; Chen, Z. Mini-LED and micro-LED. Promising candidates for the next generation display technology. *Appl. Sci.* **2018**, *8*, 1557. [CrossRef]
7. Mukai, T.; Yamada, M.; Nakamura, S. Characteristics of InGaN-based UV/blue/green/amber/red light-emitting diodes. *Jpn. J. Phys.* **1999**, *38*, 3976–3981. [CrossRef]
8. Chitnis, A.; Kumar, A.; Shatalov, M.; Advarahan, V.; Lunev, A.; Yang, J.W.; Simin, G.; Gaska, R.; Shur, M. High quality p-n junctions with quaternary AlInGaN/InGaN quantum wells. *Appl. Phys. Lett.* **2000**, *77*, 3800–3802. [CrossRef]

9. Lee, S.N.; Paek, H.S.; Kim, H.; Jang, T.; Park, Y. Monolithic InGaN-based white light-emitting diodes with blue, green and amber emissions. *Appl. Phys. Lett.* **2008**, *92*, 081107. [CrossRef]
10. Teng, C.H.; Zhang, L.; Deng, H.; Ku, P.C. Strain-induced red-green-blue wavelength tuning in InGaN quantum wells. *Appl. Phys. Lett.* **2016**, *108*, 071104. [CrossRef]
11. Li, H.; Li, P.; Kang, J.; Li, Z.; Li, J.; Yi, X.; Wang, G. Phosphor-free color-tunable monolithic InGaN light-emitting diodes. *Appl. Phys. Exp.* **2013**, *6*, 102103. [CrossRef]
12. Ho, I.H.; Stringfellow, G.B. Solid phase immiscibility in GaInN. *Appl. Phys. Lett.* **1996**, *22*, 2701–2703. [CrossRef]
13. McCluskey, M.D.; Romano, L.T.; Krusor, B.S.; Bour, D.P.; Johnson, N.M. Phase sparation in InGaN/GaN multiquantum wells. *Appl. Phys. Lett.* **1998**, *72*, 1730–1732. [CrossRef]
14. Hao, M.; Ishikawa, H.; Egawa, T.; Shao, C.L.; Jimbo, T. Anomalous compositional pulling effect in InGaN/GaN multiple quantum wells. *Appl. Phys. Lett.* **2003**, *82*, 4702–4704. [CrossRef]
15. Chung, W.; Jung, H.; Lee, C.H.; Kim, S.H. Fabrication of high color rendering index white LED using Cd-free wavelength tunable Zn doped $CuInS_2$ nanocrystal. *Opt. Exp.* **2012**, *20*, 25071–25076. [CrossRef]
16. Pimputkar, S.; Speck, J.S.; DenBaars, S.P.; Nakamura, S. Prospects for LED lighting. *Nat. Photon.* **2009**, *3*, 180–182. [CrossRef]
17. Sun, C.C.; Chen, C.Y.; He, H.Y.; Chen, C.C.; Chien, W.T.; Lee, T.X.; Yang, T.H. Precise optical modeling for silicate-based white LEDs. *Opt. Exp.* **2008**, *16*, 20060–20066. [CrossRef]
18. Nizamoglu, S.; Ozel, T.; Sari, E.; Demir, H.V. White light generation using CdSe/ZnS core-shell nanocrystals hybridized with InGaN/GaN light emitting diodes. *Nanotechnology* **2007**, *18*, 065709. [CrossRef]
19. Ma, Z.; Li, X.; Zhang, C.; Turyanska, L.; Lin, S.; Xi, X.; Li, H.; Hu, T.; Wang, J.; Patane, A.; et al. CsPb(Br/I)3 perovskite nanocrystals for hybrid GaN-based high-bandwidth white light-emitting diode. *ACS Appl. Nano Mater.* **2021**, *4*, 8383–8389. [CrossRef]
20. Zhang, C.; Zhu, X.; Gao, F.; Yang, L.; Liu, W. Stable white emission and color tunable electroluminescence achieved from n-ZnO/p-GaN nano-heterojunction decorated with CsPbBr3 and CsPbI3 quantum dots. *J. Lumin.* **2022**, *244*, 118691. [CrossRef]
21. Yan, D.; Zhao, S.; Zhang, Y.; Wang, H.; Zang, Z. High efficient emission and high-CRI warm white light-emission diode form ligand-modified $CsPbBr_3$ quantum dots. *Opto-Electron. Adv.* **2022**, *5*, 200075. [CrossRef]
22. Zheng, C.; Bi, C.; Huang, F.; Binks, D.; Tian, J. Stable and strong emission $CsPbBr_3$ quantum dots by surface engineering for high-performance optoelectronic films. *ACS Appl. Mater. Interfaces* **2019**, *11*, 25410–25416. [CrossRef]
23. Cho, S.B.; Sohn, J.I.; Lee, S.S.; Moon, S.G.; Hou, B.; Park, I.K. Colour-encoded electroluminescent white light-emitting diodes enabled using perovskite–Cu–In–S quantum composites. *J. Mater. Chem. C* **2021**, *9*, 7027–7034. [CrossRef]
24. Xi, Y.; Schubert, E.F. Junction-temperature measurement in GaN ultraviolet light-emitting diodes using diode forward voltage method. *Appl. Phys. Lett.* **2004**, *85*, 2163–2165. [CrossRef]
25. Ji, Y.; Wang, M.; Yang, Z.; Qiu, H.; Ji, S.; Dou, J.; Gaponenko, N.V. Highly stable Na. $CsPb(Br,I)_3@Al_2O_3$ nanocomposites prepared by a pre-protection strategy. *Nanoscale* **2020**, *12*, 6403–6410. [CrossRef]
26. Chichibu, S.F.; Abare, A.C.; Minsky, M.S.; Keller, S.; Fleischer, S.B.; Bowers, J.E.; Hu, E.; Mishra, U.K.; Coldren, L.A.; DenBaars, S.P. Effective band gap inhomogeneity and piezoelectric field in InGaN/GaN multiqunatum well structure. *Appl. Phys. Lett.* **1998**, *73*, 2006–2008. [CrossRef]
27. Lee, S.N.; Paek, H.S.; Son, J.K.; Sakong, T.; Nam, O.H.; Park, Y. Characteristics of Si and Mg doping in a-plane GaN grown on r-plane sapphire. *J. Cryst. Growth* **2007**, *307*, 358–362. [CrossRef]
28. Lv, W.; Li, L.; Xu, M.; Hong, J.; Tang, X.; Xu, L.; Wu, Y.; Zhu, R.; Chen, R.; Huang, W. Improving the stability of metal halide perovskite quantum dots by encapsulation. *Adv. Mat.* **2019**, *31*, 1900682. [CrossRef]
29. Yuan, X.; Hou, X.; Li, J.; Qu, C.; Zhang, W.; Jhao, J.; Li, H. Thermal degradation of luminescence in inorganic perovskite $CsPbBr_3$ nanocrystals. *Phys. Chem. Chem. Phys.* **2017**, *19*, 8934–8940. [CrossRef]
30. Keppens, A.; Ryckeart, W.R.; Deconinck, G.; Hanselaer, P. High power light-emitting diode junction temperature determination from current-voltage characteristics. *J. App. Phys.* **2008**, *104*, 093104. [CrossRef]
31. Lu, T.; Ma, Z.; Du, C.; Fang, Y.; Wu, H.; Jiang, Y.; Wang, L.; Dai, L.; Jia, H.; Liu, W.; et al. Temperature-dependent photoluminescence in light-emitting diodes. *Sci. Rep.* **2014**, *4*, 6131. [CrossRef] [PubMed]
32. Wang, J.C.; Fang, C.H.; Wu, Y.F.; Chen, W.J.; Kuo, D.C.; Fan, P.L.; Jiang, J.A.; Nee, T.E. The effect of junction temperature on the optoelectrical properties of InGaN/GaN multiple quantum well light-emitting diodes. *J. Lumin.* **2012**, *132*, 429–433. [CrossRef]
33. Franssen, G.; Litwin-Staszewska, E.; Piotrzkowski, R.; Suski, T.; Perlin, P. Optical and electrical properties of homoepitaxially grown multiquantum well InGaN/GaN light-emitting diodes. *J. Appl. Phys.* **2003**, *94*, 6122–6128. [CrossRef]
34. Buso, S.; Spiazzi, G.; Meneghini, M.; Meneghesso, G. Performance degradation of high-brightness light emitting diodes under DC and pulsed bias. *IEEE Trans. Dev. Mat. Reliabl.* **2008**, *8*, 312–322. [CrossRef]